

Diffusion Model for GPS Trajectory Generation

Yuanshao Zhu^{*†}, Yongchao Ye^{*}, Xiangyu Zhao[†], and James J.Q. Yu^{*}

^{*} Southern University of Science and Technology

[†]City University of Hong Kong

Abstract—With the deployment of GPS-enabled devices and data acquisition technology, the massively generated GPS trajectory data provide a core support for advancing spatial-temporal data mining research. Nonetheless, GPS trajectories comprise personal geo-location information, rendering inevitable privacy concerns on plain data. One promising solution to this problem is trajectory generation, replacing the original data with the generated privacy-free ones. However, owing to the complex and stochastic behavior of human activities, generating high-quality trajectories is still in its infancy. To achieve the objective, we propose a **diffusion-based trajectory generation (Diff-Traj)** framework, effectively integrating the generation capability of the diffusion model and learning from the spatial-temporal features of trajectories. Specifically, we gradually convert real trajectories to noise through a forward trajectory noising process. Then, Diff-Traj reconstructs forged trajectories from the noise by a reverse trajectory denoising process. In addition, we design a **trajectory UNet (Traj-UNet)** structure to extract trajectory features for noise level prediction during the reverse process. Experiments on two real-world datasets show that Diff-Traj can be intuitively applied to generate high-quality trajectories while retaining the original distribution.

Index Terms—Diffusion model, Privacy preserving, Spatial-temporal data mining, GPS trajectory

1 INTRODUCTION

GPS trajectory data underlie a wide range of spatial-temporal data mining studies, such as urban traffic planning, business location selection, and travel time estimation [1], [2], [3]. Since trajectories are closely associated with personal geo-location, supporting downstream tasks by directly exploiting real-world trajectories inevitably leads to privacy concerns [4], [5]. Therefore, it is an urgent issue to serve these urban applications while protecting the personal privacy of the original data. Fig. 1 illustrates an intuitive solution for this issue: generate trajectories by learning the real trajectory distribution, and replace the real trajectory that contains personal privacy with the forged ones [6], [7], [8]. Based on the generated trajectories, one can expect to achieve an equivalent outcome from data analysis and support upper-level business construction while avoiding privacy leakage.

However, generating trajectories with real-world distribution encounters the following challenges in practice. Firstly, different regions within a city serve diverse functions and population densities, which leads to the non-independent and identical distribution (non-iid) nature of trajectories among regions [5], making it challenging to learn the trajectory distribution globally. In addition, trajectories are unique as human activities are inherently stochastic, rendering the modeling of trajectories challenging. Lastly, external factors (traffic conditions, departure time, etc.) play a non-negligible role in personal mobility, rendering the correlation of individual GPS locations within a trajectory challenging to model explicitly.

To address the above challenges, a number of trajectory generation efforts have been proposed. For example, several studies suggested generating trajectories for the next period based on previous trajectories (also called trajectory prediction) [6], [9], [10], [11]. However, such approaches require using real-world trajectories for prediction, which fails to comply with the privacy preservation objective. Another option is to divide the city into

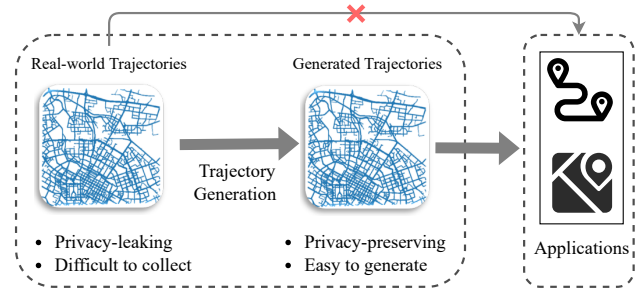


Fig. 1. Intuition of trajectory generation. Trajectories are generated by learning real-world trajectory distributions and serving downstream applications with privacy-free ones.

multiple grids and perform trajectory generation by learning the distribution of trajectories within grids [4], [12]. Nevertheless, it is hard to balance the trade-off between grid size and distribution accuracy. Furthermore, utilizing the superior image generation capability by generative adversarial networks (GAN), researchers transform trajectories into images of GPS points and generate new ones by GAN [13], [14]. However, such GAN-based approaches require image-to-trajectory and trajectory-to-image translation, which imposes additional computation and notable translation error. In addition, it is difficult to obtain satisfactory results due to unstable training. Despite the persistent efforts of the aforementioned studies in trajectory generation tasks, existing research remains deficient. In practice, an effective promising trajectory generation solution should be able to protect privacy, produce satisfactory accuracy, and prevent excessive computational overhead.

To bridge this research gap, we propose a trajectory generation method based on the diffusion model, which can model various complex behaviors of real world activities and generate high-quality trajectories. The core idea of the diffusion model is to use the forward trajectory diffusion process to perturb the trajectory

distribution with noise and then recover the trajectory distribution by learning the backward diffusion process (denoising), yielding a highly flexible and easy-to-compute trajectory generation model [15], [16]. We propose this framework based on three primary motivations: (i) The diffusion model is a more reliable and robust method of generation than canonical methods [17]. (ii) Human activities in the real world are stochastic and uncertain [18], while the diffusion model reconstructs the data step-by-step from random noise, making it applicable to generate more realistic GPS trajectories. (iii) The diffusion model generates trajectories from random noise, which is free from the risk of privacy leakage.

Following these motivations, we propose a **Diffusion model Trajectory generation (Diff-Traj)** framework, which can generate a large number of trajectories and maintain the real-world trajectory distribution. Diff-Traj performs spatial-temporal modeling of the raw trajectory without additional operations, allowing it to be applied directly for trajectory generation. Essentially, the forged trajectories generated by Diff-Traj guarantee the generation accuracy while retaining the utility. To summarize, the primary contributions of this work are concluded as follows:

- We propose a framework for trajectory generation based on the diffusion model, which can simulate real-world trajectory and generate high-quality trajectory data. To the best of our knowledge, this is a pioneering work on trajectory generation by the diffusion model.
- We design a novel neural network structure called Traj-UNet, which integrates the residual block and attention mechanism to model fine-grained spatial-temporal features in trajectories.
- We validate the effectiveness of Diff-Traj on two real-world trajectory datasets, and the experimental results show that the proposed framework can generate realistic trajectories according well with real-world distributions and retain data utility.

The rest of this paper is organized as follows. Section 2 provides preliminary definitions and formalizes the problem to be addressed in this work. Then, Section 3 elaborates on the proposed Diff-Traj framework, including the structure of Traj-UNet and essential principles of the diffusion model. Section 4 conducts a series of experiments on two real-world trajectory datasets to assess the performance of the proposed framework. Next, we review the literature on trajectory generation and diffusion models in Section 5. Finally, we conclude this paper in Section 6.

2 PRELIMINARY

In this section, we first briefly introduce the fundamentals of trajectory generation and then formulate the objective of the problem.

Definition 1: (GPS Trajectory) Given a real-world GPS trajectory, it consists of a sequence of continuously sampled private GPS location points, denoted by $\mathbf{x} = \{p_1, p_2, \dots, p_n\}$. The i -th GPS point is represented as a tuple $p_i = [\text{lat}_i, \text{lng}_i]$, where lng_i and lat_i denote longitude and latitude, respectively.

Definition 2: (Jensen-Shannon Divergence) Jensen-Shannon Divergence (JSD) is a common metric of divergence, which quantifies the degree of difference between two distributions. Suppose that the original data has a probability distribution P

and the generated data has a probability distribution G , the JSD is calculated as follows:

$$\text{JSD}(P\|G) = \frac{1}{2}\mathbb{E}_P \left[\log \frac{P}{P+G} \right] + \frac{1}{2}\mathbb{E}_G \left[\log \frac{G}{G+P} \right]. \quad (1)$$

The above equation shows that JSD is symmetric and takes values in the range $[0, 1]$. A smaller JSD means it is more indistinguishable between two distributions, and $\text{JSD} = 1$ denotes no correlation.

Problem 1: (Trajectory Generation) Based on real-world trajectory datasets, the trajectory generation task can be defined as a sequential decision process. In other words, it is described as the product of the probabilities of each generated GPS point:

$$G(\hat{\mathbf{x}}) = \prod_{i=1}^n \text{Pr}_\theta(\hat{p}_i \mid \hat{p}_1, \dots, \hat{p}_{i-1}), \quad (2)$$

where Pr_θ denotes the generated probability distribution of the parametric generator G and $\hat{\mathbf{S}} = \{\hat{p}_1, \hat{p}_2, \dots, \hat{p}_n\}$ is the generated GPS trajectory. Therefore, the objective of trajectory generation is to generate replaceable trajectories, which minimize the JSD between the original $P(\mathbf{S})$ and generated $G(\hat{\mathbf{x}})$ trajectory:

$$\underset{\theta}{\text{minimize}} \quad \text{JSD}(P(\mathbf{x}) \parallel G(\hat{\mathbf{x}})). \quad (3)$$

In practice, $P(\mathbf{x})$ and $G(\hat{\mathbf{x}})$ may have various physical meanings, such as the regional distribution of trajectory points, the distance between successive points, etc.

3 METHODOLOGY

In this section, we elaborate on the proposed Diff-Traj. We start by presenting the fundamentals of the diffusion model, including two main processes, objective optimization function, and sampling speed-up methods. Then, we introduce the details of the denoising model, i.e., Traj-UNet.

3.1 Diff-Traj Framework

As shown in Fig. 2, the Diff-Traj framework involves two main processes, namely, the forward trajectory noising process and the reverse trajectory denoising process. The former aims to iteratively add noise to the trajectory sequence that ultimately converges into a Gaussian distribution. The latter subsequently reconstructs the Gaussian noise for each step and eventually generates the GPS trajectory sequence [15], [16], [17]. At each step in the reverse trajectory denoising process, the noise is predicted by a designed neural network called Traj-UNet.

3.1.1 Forward Trajectory Noising Process

This process involves introducing noise to the initial trajectory while simultaneously learning its spatial-temporal features. Since noise is stochastically created, it requires careful tuning to make sure that the resulting trajectories are realistic and free of any irrational behavior. Additionally, this process requires an incremental approach to prevent excessive noise from severely biasing the trajectory or impairing the precision of its creation.

To address above challenges, the forward process can be considered as step-wise noisifying the trajectory. Given a real-world trajectory sample $\mathbf{x} \sim q(\mathbf{x})$, the forward process adds T time-steps of Gaussian noise to it, where T is an adjustable parameter. Subsequently, each step holds a noise trajectory and obtains a set of noisy trajectories $\{\mathbf{x}_0, \mathbf{x}_1, \dots, \mathbf{x}_T\}$. In practice,

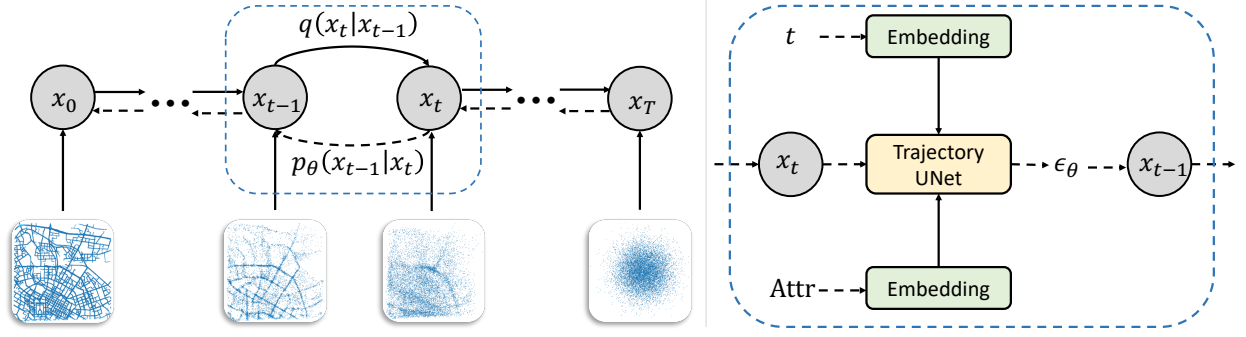


Fig. 2. The proposed framework for trajectory generation. (Left) Diffusion model process, which is divided into a forward noising process and the reverse denoising process. (Right) An illustration of the model structure for reverse denoising.

we consider the x_0 indicates the raw trajectory without any manipulation. x_t loses its spatial-temporal features as t increases and finally converges into a unit Gaussian $x_T \sim \mathcal{N}(0, \mathbf{I})$. Since it is a step-by-step chain calculation, we can express it as a Markov process:

$$q(x_t | x_{t-1}) = \mathcal{N}(x_t; \sqrt{1 - \beta_t}x_{t-1}, \beta_t \mathbf{I})$$

$$q(x_{1:T} | x_0) = \prod_{t=1}^T q(x_t | x_{t-1}), \quad (4)$$

where $\mathcal{N}(\cdot)$ denotes Gaussian noise and $\{\beta_t \in (0, 1)\}_{t=1}^T$ ($\beta_1 < \beta_2 < \dots < \beta_T$) is the corresponding variance schedule. Let $\alpha_t = 1 - \beta_t$ and $\bar{\alpha}_t = \prod_{i=1}^t \alpha_i$. Since it is impractical to backpropagate the gradient by sampling from a Gaussian distribution, we adopt a reparameterization trick to keep the gradient derivable [15]. Specifically, sampling $z \sim \mathcal{N}(z; \mu, \sigma^2 \mathbf{I})$ from the standard Gaussian distribution can be formulated as:

$$z = \mu_\theta + \sigma_\theta \odot \epsilon, \quad \epsilon \sim \mathcal{N}(0, \mathbf{I}), \quad (5)$$

where \odot indicates element-wise product. According to this trick, x_t can be written as:

$$x_t = \sqrt{\alpha_t}x_{t-1} + \sqrt{1 - \alpha_t}\epsilon_{t-1}$$

$$= \sqrt{\alpha_t\alpha_{t-1}}x_{t-2} + \sqrt{1 - \alpha_t\alpha_{t-1}}\bar{\epsilon}_{t-2}$$

$$= \dots$$

$$= \sqrt{\bar{\alpha}_t}x_0 + \sqrt{1 - \bar{\alpha}_t}\epsilon, \quad (6)$$

where $\epsilon_t \sim \mathcal{N}(0, \mathbf{I})$ and $\bar{\epsilon}_t$ is the aggregation of two Gaussian distributions. Then, Eq. (4) can be rewritten as:

$$q(x_t | x_0) = \mathcal{N}(x_t; \sqrt{\bar{\alpha}_t}x_0, (1 - \bar{\alpha}_t)\mathbf{I}). \quad (7)$$

As a result, we can sample from a Gaussian at any time step to obtain the noisy trajectory x_t . During this process, a tailored deep neural network is applied to learn the spatial-temporal characteristics of the corresponding noise level.

3.1.2 Reverse Trajectory Denoising Process

This process takes Gaussian noise as the input and infers the forged trajectory. During this process, the most challenging point is estimating the noise level from the noisy input trajectory.

To tackle this challenge, in practice, we can implement the denoising process in a stepwise $x_t \rightarrow x_{t-1}$ manner. Since estimating the reverse conditional probability $q(x_{t-1} | x_t)$ is

intractable [15], [16], which can use a parameterized neural network p_θ to approximate this process:

$$p_\theta(x_{t-1} | x_t) = \mathcal{N}(x_{t-1}; \mu_\theta(x_t, t), \Sigma_\theta(x_t, t)),$$

$$p_\theta(x_{0:T}) = p_\theta(x_T) \prod_{t=1}^T p_\theta(x_{t-1} | x_t), \quad (8)$$

where $\mu_\theta(x_t, t)$ and $\Sigma_\theta(x_t, t)$ are the mean and variance, respectively. With the Bayesian formula, the reverse conditional probability can be derived when conditioned on x_0 :

$$q(x_{t-1} | x_t, x_0) = \mathcal{N}(x_{t-1}; \tilde{\mu}_t(x_t, x_0), \tilde{\beta}_t \mathbf{I}), \quad (9)$$

where

$$\tilde{\mu}_t(x_t, x_0) = \frac{\sqrt{\bar{\alpha}_{t-1}}\beta_t}{1 - \bar{\alpha}_t}x_0 + \frac{\sqrt{\alpha_t}(1 - \bar{\alpha}_{t-1})}{1 - \bar{\alpha}_t}x_t$$

$$\tilde{\beta}_t = \frac{1 - \bar{\alpha}_{t-1}}{1 - \bar{\alpha}_t}\beta_t. \quad (10)$$

Based on Eq. (6), replacing Eq. (10) with $x_0 = \frac{1}{\sqrt{\bar{\alpha}_t}}(x_t - \sqrt{1 - \bar{\alpha}_t}\epsilon)$, we have:

$$\tilde{\mu}_t = \frac{1}{\sqrt{\alpha_t}}\left(x_t - \frac{1 - \alpha_t}{\sqrt{1 - \bar{\alpha}_t}}\epsilon\right). \quad (11)$$

Here, the Gaussian distribution ϵ is the noise predicted by the neural network model (for denoising), i.e., $\epsilon_\theta(x_t, t)$, which gives:

$$\mu_\theta(x_t, t) = \frac{1}{\sqrt{\alpha_t}}\left(x_t - \frac{\beta_t}{\sqrt{1 - \bar{\alpha}_t}}\epsilon_\theta(x_t, t)\right). \quad (12)$$

For convenience of calculation, $\Sigma_\theta(x_t, t) = \sigma_t^2 \mathbf{I}$ and σ_t^2 is approximated by the variance $\tilde{\beta}_t$.

In conclusion, the reverse trajectory denoising process can be summarized as learning the Gaussian noise $\epsilon_\theta(x_t, t)$ through x_t and t , and then solving $\mu_\theta(x_t, t)$ according to Eq. (12). The stepwise denoising process is expressed as following equation:

$$p_\theta(x_{t-1} | x_t) = \mathcal{N}\left(x_{t-1}; \frac{1}{\sqrt{\alpha_t}}\left(x_t - \frac{1 - \alpha_t}{\sqrt{1 - \bar{\alpha}_t}}\epsilon_\theta(x_t, t)\right), \tilde{\beta}_t \mathbf{I}\right). \quad (13)$$

Therefore, we can finally forge real-world-like trajectory data from random Gaussian with trained forward and backward processes.

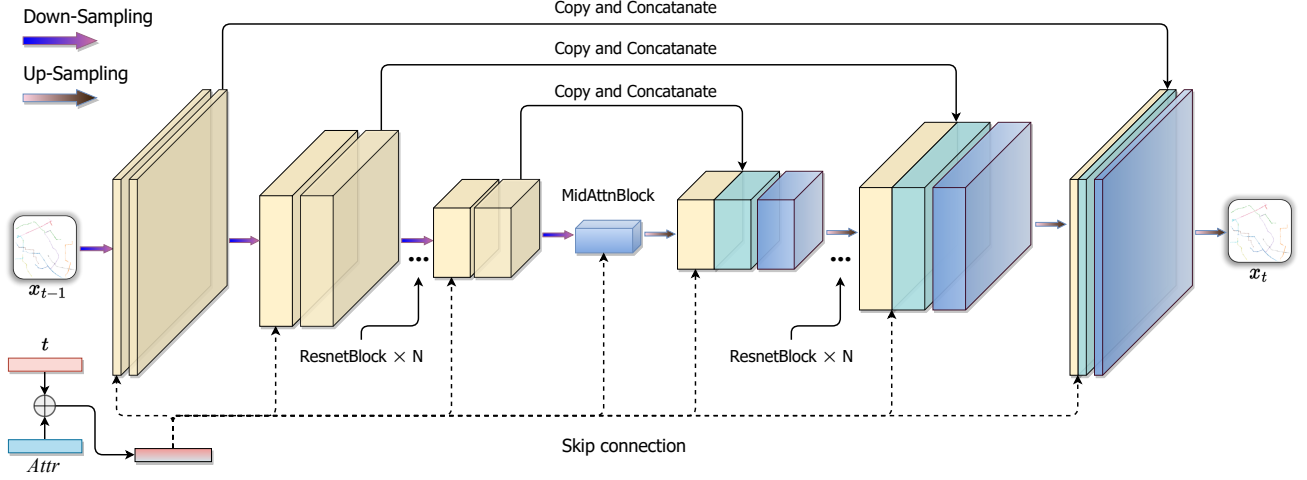


Fig. 3. The structure of Traj-UNet is divided into two modules, down-sampling and up-sampling, each of which contains multiple Resnet blocks. For each Resnet block, the time step and external attribute embedding are integrated.

3.1.3 Objective Optimization Function

Recall that we need to approximate the conditional probability distribution $p_\theta(x_{t-1} | x_t)$ in the reverse trajectory denoising process. A typical method is to design a parameterized neural network model to predict the $\epsilon_\theta(x_t, t)$ and implement this process by Eq. (13).

Since Diff-Traj contains two multi-step iteration processes, the design of the objective optimization function should guarantee desired results and is computationally efficient. Thus, the objective optimization function can be derived by maximizing the log-likelihood between the predicted and original distributions, as follows.

$$\mathcal{L} = \mathbb{E}_{q(x_0)} [-\log p_\theta(x_0)] . \quad (14)$$

Similarly, the above formula can be optimized for negative log-likelihood by obtaining the variational lower bound based on variational inference [15]:

$$\begin{aligned} \mathcal{L} &\leq \mathbb{E}_q \left[-\log \frac{p_\theta(x_{0:T})}{q(x_{1:T} | x_0)} \right] \\ &\propto \mathbb{E}_q \left[\sum_{t=2}^T D_{KL}(q(x_{t-1} | x_t, x_0) \| p_\theta(x_{t-1} | x_t)) \right] . \end{aligned} \quad (15)$$

Therefore, the objective optimization function simplifies to:

$$\begin{aligned} \mathcal{L} &= \mathbb{E}_{x_0, \epsilon} \left[\frac{1}{2 \|\Sigma_\theta(x_t, t)\|^2} \|\tilde{\mu}_t(x_t, x_0) - \mu_\theta(x_t, t)\|^2 \right] \\ &= \mathbb{E}_{x_0, \epsilon} \left[\frac{\beta_t^2}{2\sigma_t^2 \alpha_t (1 - \bar{\alpha}_t)} \|\epsilon - \epsilon_\theta(\sqrt{\bar{\alpha}_t}x_0 + \sqrt{1 - \bar{\alpha}_t}\epsilon, t)\|^2 \right] \\ &\propto \mathbb{E}_{t, x_0, \epsilon} \left[\|\epsilon - \epsilon_\theta(\sqrt{\bar{\alpha}_t}x_0 + \sqrt{1 - \bar{\alpha}_t}\epsilon, t)\|^2 \right] . \end{aligned} \quad (16)$$

The above equations show that the core of optimizing the diffusion model is to minimize the mean squared error between the Gaussian noise ϵ and predicted ϵ_θ .

We give a detailed description of the optimization for Diff-Traj in Algorithm 1. We start by sampling a mini-batch real-world trajectories (line 2); next, we sample t and ϵ from a uniform distribution and the standard Gaussian distribution, respectively (line 3); subsequently, we calculate the objective function \mathcal{L} in

Algorithm 1: The Optimization for Diff-Traj.

Input: Trajectories dataset $x \in \mathcal{D}$

Output: Well-learned parameters of θ^*

- 1: **while** not converged **do**
 - 2: Sample a mini-batch of trajectories $x_0 \sim q(x)$
 - 3: $t \sim \text{Uniform}\{1, \dots, T\}$ and $\epsilon \sim \mathcal{N}(0, \mathbf{I})$
 - 4: Calculate the objective via Eq. (16)
 - 5: Update θ by descending $\nabla_\theta \mathcal{L}$
 - 6: **end while**
-

Eq. (16) (line 4); and finally, θ is updated via descending $\nabla_\theta \mathcal{L}$ (line 5). The above steps are iterated until the objective function converges.

3.1.4 Speed up Diffusion Model Sampling

As described in Sec. 3.1.1 and Sec. 3.1.2, Diff-Traj relies on a large Markov process to generate high-quality trajectories, rendering a slow reverse diffusion process. To address this issue, literature [16] proposed a non-Markov diffusion process method with the same optimization objective, thus allowing a computationally efficient reverse process. Specifically, following the reparameterization approach in Eq. (5) and Eq. (4), we have

$$\begin{aligned} x_{t-1} &= \sqrt{\bar{\alpha}_{t-1}}x_0 + \sqrt{1 - \bar{\alpha}_{t-1}}\epsilon_{t-1} \\ &= \sqrt{\bar{\alpha}_{t-1}}x_0 + \sqrt{1 - \bar{\alpha}_{t-1} - \sigma_t^2}\epsilon_t + \sigma_t\epsilon \\ &= \sqrt{\bar{\alpha}_{t-1}}x_0 + \sqrt{1 - \bar{\alpha}_{t-1} - \sigma_t^2} \frac{x_t - \sqrt{\bar{\alpha}_t}x_0}{\sqrt{1 - \bar{\alpha}_t}} + \sigma_t\epsilon . \end{aligned} \quad (17)$$

Then, we can sample every $\lceil T/S \rceil$ steps with the skip-step method presented in [19]. The corresponding set of noise trajectories changes to $\{\tau_1, \dots, \tau_S\}$, $\tau_i \in [1, T]$. Through this approach, the sampling steps during trajectory generation can be significantly reduced from T steps to S steps. Therefore, the reverse denoising process of Eq. (9) is rewritten as:

$$\begin{aligned} q_{\sigma, \tau}(x_{\tau_i-1} | x_t, x_0) \\ = \mathcal{N}(\sqrt{\alpha_{t-1}}x_0 + \sqrt{1 - \alpha_{t-1} - \sigma_t^2} \frac{x_{\tau_i} - \sqrt{\alpha_t}x_0}{\sqrt{1 - \alpha_t}}, \sigma_t^2 \mathbf{I}) . \end{aligned} \quad (18)$$

Unlike Eq. (7) and Eq. (12), Eq. (18) introduces variance σ_t^2 into the mean of Gaussian. Let $\sigma_t^2 = \eta \hat{\beta}_t$, where $\eta \in \mathbb{R}$ is a hyperparameter that controls sampling randomness. In such a case, Eq. (18) is equivalent to Eq. (7) when $\eta = 1$, i.e., $\sigma_t^2 = \hat{\beta}_t = \frac{1-\alpha_t-1}{1-\alpha_t} \beta_t$. On the other hand, the sampling process of diffusion loses all randomness to obtain a deterministic result when $\eta = 0$. Compared to the typical diffusion model [15], this method can generate higher quality samples in fewer steps [16].

3.2 Coupled Traj-UNet for Denoising

In Sec. 3.1, we have introduced the theoretical foundation of Diff-Traj framework, i.e., the forward trajectory noising and reverse trajectory denoising processes. In this section, we present the proposed neural network model to learn the noise ϵ_θ , assisting the reverse trajectory denoising process. Typically, the denoising network for the diffusion model follows the UNet structure [17], [20], with the input being the time step t and the corresponding noise sample, and outputting Gaussian noise corresponding to \mathbf{x}_t . Unlike the traditional structure presented in [20], Traj-UNet incorporates time steps and traffic contextual information for each down/up-sampling blocks, as well as 1D convolutions to capture fine-grained spatio-temporal features. As illustrated in Fig. 3, Traj-UNet is divided into two modules, i.e., down-sampling and up-sampling, each consisting of multiple stacked Resnet blocks. Between the two modules, a transitional module based on the attention mechanism is integrated [21]. To better learn the noise of each time step, Traj-UNet embeds the time step and external traffic information, later fed to each block.

3.2.1 Component Blocks

As previously stated, Traj-UNet consists of several blocks with different architectures and functionalities. We first detail the role and design of each block depicted in Fig. 4.

Sampling Block. This is the most essential component of Traj-UNet. As illustrated in Fig. 3, the sampling blocks (both down- and up-sampling) consists of multiple Resnet blocks, each containing a series of group normalization, nonlinear activation, and 1D convolutional layers. For a given input $\mathbf{X} \in \mathbb{R}^{c \times n}$ (c and n represent the dimensions and length of the acquired trajectory features, respectively), the Resnet block can be formulated as:

$$\begin{aligned} \mathbf{X}^l &= \text{Conv}(\sigma(\text{GN}(\mathbf{X}^{l-1}))), \\ \mathbf{X}^l &= \mathbf{X}^l + \text{Concat}(\text{Embed}(t), \text{Embed}(Attr)), \\ \mathbf{X}^l &= \text{Conv}(\sigma(\text{GN}(\mathbf{X}^l))), \\ \mathbf{X}^l &= \mathbf{X}^l + \mathbf{X}^{l-1}, \end{aligned} \quad (19)$$

where $\sigma(\cdot)$ is the nonlinear activation function. For each Resnet block, we use a skip connection to join the output of the convolutional layer with the input features from the same level. This design permits the model to capture spatial-temporal features at different resolutions and skip connections to facilitate the addition of trajectory details. After this, Traj-UNet applies up-sampling or down-sampling to the output, where down-sampling uses maximum-pooling and up-sampling uses interpolation.

Middle Attention Block. After the capture spatial-temporal features capturing by down- and up-sampling modules, Traj-UNet needs to determine the importance of its high-dimensional features to improve the accuracy and efficiency of the generation process. To address this issue, Traj-UNet integrates a middle attention block. As shown in Fig. 4, it consists of two Resnet blocks

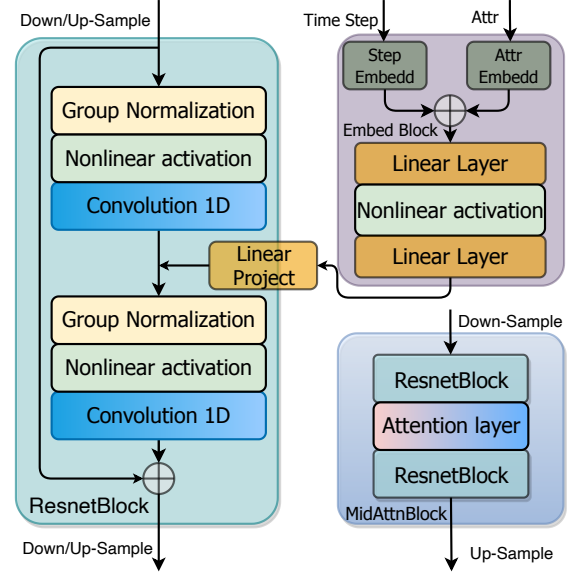


Fig. 4. The main components of Traj-UNet including Resnet block, embed block, attention layer, and middle attention block.

and an attention layer. Note that there are no additional down/up-sampling operations in the Resnet block. In Traj-UNet, the attention layer can be formulated as follows:

$$\begin{aligned} \text{Attention}(\mathbf{Q}, \mathbf{K}, \mathbf{V}) &= \text{softmax}\left(\frac{\mathbf{Q}\mathbf{K}^\top}{\sqrt{d}}\right) \cdot \mathbf{V}, \\ \mathbf{X}^{l+1} &= \mathbf{X}^l + \text{Attention}(\mathbf{Q}, \mathbf{K}, \mathbf{V}), \end{aligned} \quad (20)$$

where $\mathbf{Q} = \mathbf{W}_Q^l \cdot \mathbf{X}^l$, $\mathbf{K} = \mathbf{W}_K^l \cdot \mathbf{X}^l$, $\mathbf{V} = \mathbf{W}_V^l \cdot \mathbf{X}^l$ (\mathbf{W}_Q , \mathbf{W}_K , and \mathbf{W}_V are learnable parameter matrices).

The motivation of this design is to first use the Resnet block to learn the high-dimensional spatio-temporal features after down-sampling. The subsequent calculation of the feature importance through attention ensures that data are propagated with efficacy. Finally, Traj-UNet integrates this information with a Resnet block to facilitate the subsequent up-sampling module.

3.2.2 Time Step and External Attribute Embedding

Encoding time step t in Diff-Traj is necessary, which is because the diffusion model generates trajectories using a probabilistic approach, requiring it to consider the current state of the trajectory at each time step. In this work, we encode each t using a 128-dimensional vector according to the method in literature [21]. We then apply two fully connected layers on the encoding and superimpose the result to the input of each Resnet block:

$$t_{\text{emb}} = \text{FC}(\sigma(\text{FC}(\text{SinTimeEmb}(t)))), \quad (21)$$

where FC denotes fully connected layer and SinTimeEmb is the step index encoding following [21].

In addition, external attributes have a non-negligible impact on the dynamics of the GPS trajectory [22], [23]. We consider the effects of travel distance, average move distance, and the departure time of the trajectory. Specifically, we adopt linear transformations with biases to embed categorical features x (i.e., departure time) into low-dimensional vectors of \mathbb{R}^{128} . Here, we divide the departure time during the day into 288 slices (5 min for each time window). For the travel distance and average move

distance, we apply the z-score for normalization. After obtaining all external attribute embedding, a fully connected layer is adopted to map them to the same dimensions of the time step embedding for data aggregation.

4 EXPERIMENTS

In this section, a series of comprehensive experiments on two real-world trajectory datasets are conducted to show the superiority of the proposed Diff-Traj. We first introduce the public datasets and evaluation metrics used in this paper. Subsequently, we briefly review selected baselines and experimental details. Finally, we analyze and discuss the result of Diff-Traj by extensive experiments.

4.1 Experimental Settings

4.1.1 Data and Configuration

We evaluate the generative performance of Diff-Traj and baselines on two real-world trajectory datasets of Chinese cities, namely, Chengdu and Xi'an. Both datasets are collected from cab trajectory data starting from November 1, 2016 to November 30, 2016. A detailed description of the dataset and statistics is available in appendix A.

4.1.2 Evaluation Metrics

As trajectory generation aims to generate trajectories that can replace real-world activities and further benefit downstream tasks, we need to evaluate the “similarity” between the forged trajectories and real ones. In this work, we follow the common practice in previous studies [8], [24] and measure the quality of the forged ones by JSD. JSD compares the distribution of the real and forged trajectories, and a lower JSD indicates a better match with the original statistical features (see Sec. 2 for details). We adopt the following metrics to evaluate the quality of the forged trajectories from four perspectives:

- **Trajectory Distribution (JS-Traj):** This metric is used to evaluate the geo-distribution between the entire forged trajectory and the real trajectory.
- **Origin Distribution (JS-O):** In addition to evaluating the trajectory distribution, this metric is adopted to assess the geo-distribution of trajectory origins.
- **Destination Distribution (JS-D):** This metric is used to evaluate the geo-distribution of trajectory destinations.
- **Travel Distance Distribution (JS-Dis):** This metric evaluates the distribution of travel distances.

In addition, since map matching is a common pre-processing step in various applications, it is essential to identify whether forged trajectories match well with the road network. Thus, the following metric is used to evaluate the quality and utility of forged trajectories:

- **Map Matching Rate (MMR):** This work adopts the fast map matching approach for map matching [25], where a higher MMR indicates that the forged trajectories are more consistent with the real-world spatial distribution of the road network and in turn human activities.

4.1.3 Implementation Details

The Diff-Traj implementation is based on PyTorch 3.7 [26], which involves various general neural network components. See appendix A for detailed hyperparameter settings and implementation details.

4.1.4 Baseline Methods

We compare Diff-Traj with two categories of baselines: non-generative and generative methods. The details of the implementation are presented in appendix A.

Non-generative:

- **Random Perturbation (RP):** Random perturbation is a method to preserve the privacy of trajectories, where each location moves in planar space at a randomly determined distance and direction.
- **Gaussian Perturbation (GP):** Gaussian perturbation is a geo-masked privacy-preserving method, where it replaces the real location with noise sampled from the Gaussian.

Generative: Please note that Diff-scatter and Diff-wo/UNet can be considered as **ablation studies** of the proposed method to evaluate the functions of the diffusion model and Traj-UNet, respectively.

- **Variational AutoEncoder (VAE):** VAE is a common data generation method, which learns data representations through an encoder and then reconstructs it by a decoder [27].
- **TrajGAN:** TrajGAN is a GAN-based framework for trajectory generation. By alternately training the generator and discriminator, it eventually enables its generated data to be consistent with the distribution of the real data [28].
- **Diff-scatter:** This method uses a diffusion model to directly generate scatter points of trajectories, which can be used to evaluate the ability of a typical diffusion model on learning citywide trajectory distribution.
- **Diff-wo/Traj-UNet:** This method is a variant of Diff-Traj without Traj-UNet, which can be used to evaluate the effectiveness of the proposed Traj-UNet spatial-temporal extraction capability.

4.2 Overall Performance

Table 1 presents the performance comparison of Diff-Traj and the selected baseline methods on two real-world datasets. Specifically, we randomly generate 1000 trajectories from each generative method and then compare their distribution with the real ones. In addition, we directly perturb the real trajectory and then calculate all metrics for each non-generative approach. Note that Diff-scatter generates scattered points and therefore cannot be applied with MMR or JS-Dis. The following conclusions can be derived from the performance comparison:

- The non-generative approaches protect privacy by perturbing the raw trajectory, but they inevitably impair the real trajectory properties. Compared to generative ones, they are inferior in all metrics. In particular, the non-generative approach demonstrates a poor result in JS-Dis due to data perturbations corrupting the motion feature within the trajectory.
- Generative methods generate trajectories directly and maintain the statistical properties of the real data. Among them, Diff-Traj achieved the best performance in all metrics. Its remarkable superiority can be attributed to the unique forward and backward diffusion processes incorporated in the model, which help better learn the distribution of trajectories. Such results advocate the employment of diffusion models in future studies related to spatial-temporal data generation. In addition, Diff-Traj significantly outperforms other methods on the JS-Dis metric,

TABLE 1
Performance Comparison of Different Approaches.

Types	Methods	Chengdu					Xi'an				
		MMR	JS-Traj	JS-O	JS-D	JS-Dis	MMR	JS-Traj	JS-O	JS-D	JS-Dis
Non-generative	RP	85.82%	0.0358	0.0245	0.0263	0.1933	51.54%	0.0157	0.0174	0.0166	0.2157
	GP	81.76%	0.0203	0.0237	0.0265	0.1918	47.35%	0.0216	0.0234	0.0213	0.1937
Generative	VAE	88.33%	0.0079	0.0070	0.0085	0.0255	67.11%	0.0131	0.0136	0.0209	0.0491
	TrajGAN	89.92%	0.0074	0.0072	0.0079	0.0285	56.64%	0.0181	0.0160	0.0198	0.0638
	Diff-scatter	—	0.0170	0.0157	0.0122	—	—	0.0267	0.0286	0.0329	—
	Diff-wo/Traj-UNet	90.72%	0.0046	0.0134	0.0161	0.0245	75.83%	0.0109	0.0219	0.0158	0.0084
	Diff-Traj	95.39%	0.0030	0.0052	0.0043	0.0071	82.15%	0.0065	0.0079	0.0076	0.0042

Bold indicates the statistically best performance (i.e., two-sided t-test with $p < 0.05$) over the best baseline.

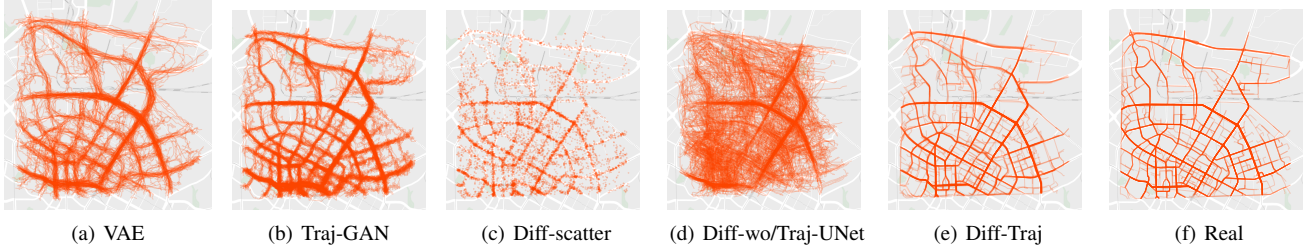


Fig. 5. Comparison of forged trajectory in Chengdu.

which indicates its ability to generate more realistic human activities.

- VAE and GAN outperform Diff-scatter and Diff-wo/Traj-UNet in some metrics, but Diff-Traj achieves optimal results when Traj-UNet is integrated. It is also noteworthy that satisfactory results can still be accomplished when using only MLP to generate scattered locations or discarding Traj-UNet structure.

Such results may be attributed to two reasons:

- 1) Traj-UNet is equipped with outstanding generation capabilities, which is able to generate trajectories consistent with the original distribution even by the simplest models and data.
- 2) Diff-Traj equipped with Traj-UNet benefits from stacking multiple Resnet blocks and skip connections, enabling it to learn spatio-temporal features and capture trajectory details at different resolutions.

To summarize, Diff-Traj relies on diffusion models and Traj-UNet to forge trajectories where the former simulates the geo-distribution of trajectories and the latter significantly improves the quality of results over existing approaches.

4.3 Geographic Visualization

In this section, we visualized the forged results to better present the performance of different generative models. Fig. 5 shows the trajectory distributions generated by baseline methods for Chengdu (The results of Xi'an are available in Fig. 11 at appendix A). Fig. 6 compares the heat map between real trajectories and forged ones. According to the results shown in Fig. 5, the trajectory data generated from VAE, Traj-GAN, and Diff-Traj are approximately identical to geo-distribution compared to original ones. Notably, the trajectories generated by Diff-Traj best resemble the road network without obvious offsets. The superior data generation

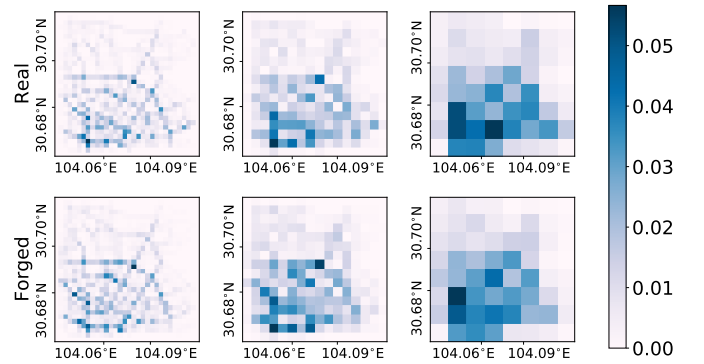
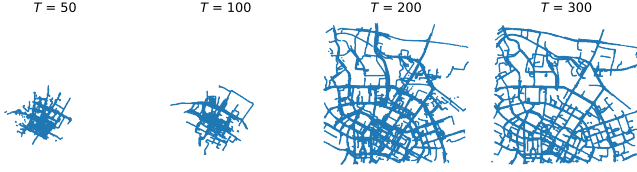


Fig. 6. Comparison of the real and forged trajectory distributions. The city is divided into different size grids (from left to right, 32×32 , 16×16 , and 8×8 grids).

capability of the diffusion model is further validated in Fig. 5(c), where the diffusion model can yield a similar distribution using only MLP to generate scattered GPS points. In addition, developing a tailor-made UNet architecture is also essential. Comparing Fig. 5(d) and Fig. 5(e), we can observe that the latter is able to generate a visually more realistic trajectory distribution. This finding can be explained by the fact that Traj-UNet is capable of recording data features in a variety of domain-specific views and resolutions, which are essential for the entire diffusion process of Diff-Traj in Sec. 3.1.

Furthermore, we visualize the heat map of the trajectory distribution with multiple resolutions. Specifically, we divide the whole city into 8×8 , 16×16 , and 32×32 grids, and then count the distribution of trajectories in each grid. The comparison clearly indicates that the distributions are highly consistent from all resolutions. The visualized results also verify the effectiveness of metrics in Table 1, revealing that the proposed model can generate high-quality trajectories with remarkable accuracy and

Fig. 7. Comparison of different diffusion steps T .

retain the original distribution.

4.4 Parameter Analysis

When designing a diffusion model, how to set the optimal diffusion step size is a common question that needs to be answered for satisfactory generation performance. In this section, we conduct experiments with Diff-Traj on two datasets to investigate the sensitivity of the diffusion process time steps T . Fig. 7 shows the performance of $T \in \{50, 100, 200, 300\}$, where we can observe that the parameter directly affects the generated results. For ($T \leq 100$), Diff-Traj suffers from too small a diffusion process (i.e., Eq. (7)), causing the trajectory generated by Diff-Traj concentrated in parts of the city. The root cause is that the trajectories are non-iid within cities (c.f. Fig. 10 in the appendix A). A small diffusion T causes the model to focus on the most important areas, ignoring the margins of the city. On the other hand, with T increases ($T \geq 200$), the results generated by Diff-Traj are shown to cover most of the area throughout the city. The results follow the widely recognized diffusion model principle that a sufficiently large diffusion step can improve its expressibility and thus utilize more significant potential features for data generation. However, the large diffusion step leads to a long sampling time during generation, which makes the Diff-Traj computationally expensive and inefficient. Therefore, Diff-Traj needs to integrate a method (presented in Sec. 3.1.4) that guarantees the generation quality while speeding up the sampling.

4.5 Speed up Sampling

As introduced in Sec. 3, the diffusion model requires a considerable sampling step to gradually denoising for generation. This is also verified by results shown in Fig. 7. In actuality, it leads Diff-Traj to generate trajectories rather slowly. Therefore, we integrate the speed-up sampling technique in Diff-Traj and examine its efficiency in this section. Specifically, through incorporating sampling speed-up technique discussed in Sec. 3.1.4, we generate 50×256 trajectories based on a well-trained Diff-Traj on two datasets.

The results are summarized in Fig. 8, where the two Y-axes represent the time spent and the JS-Traj score, respectively. Here, the total sampling step is $T = 300$ and the X-axis represents the sample steps after speed up, e.g., sampling every 6 steps if $S = 50$. We observe that all models trained with $T = 300$ diffusion steps unsurprisingly yield high-quality trajectories similar to the original distribution. In the meantime, the model manages to match the outcomes of the no skipped steps method at $T = 50$ while saving 82% of the time cost. However, too few sampling steps ($S < 50$) lead to a substantial distribution divergence between the forged trajectories and real ones. The reason is that with fewer sample steps, more reverse operations have to be skipped, rendering Diff-Traj discarding more noisy information during the denoising process. Nevertheless, this result adequately indicates the outstanding contribution of the speeding up methods (in Sec. 3.1.4) for efficiency improvement.

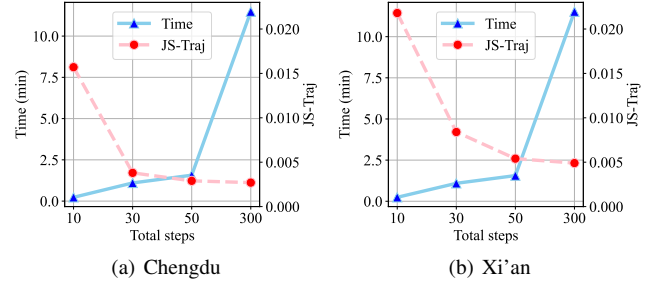


Fig. 8. Sampling Efficiency Comparison.

4.6 Utility of Generated Data

As the forged trajectories serve downstream tasks, their utility is critical to determine whether the data generation method is indeed practical. In this section, we evaluate the utility of forged trajectories through map-matching, which is a common pre-processing technique in various applications [5], [29]. Specifically, we evaluate the map-matching rate of the forged trajectories and visualize them according to the fast map-matching method [25]. As concluded in Table 1, trajectories generated by Diff-Traj achieved the best MMR scores, where the Chengdu dataset enjoys better results than Xi'an. The result is aligned with the road conditions in both cities, i.e., the roads in the Xi'an dataset are shorter and more intensive, making it challenging to match the maps. We further delve into a specific region and visualize the forged trajectories in Fig. 9, where the red dashed line indicates forged ones, and the blue dotted line indicates matched ones. Compared to other results, trajectories from Diff-Traj are more aligned with the road network, which implies a higher utility. Those compared methods may cause significant errors in map-matching and potentially undermine downstream service performance. These findings are also confirmed by Fig. 5, where Diff-Traj holds a smaller offset from roads.

5 RELATED WORK

Mobility Data Synthesizing Existing methods for protecting the privacy of trajectory data can be generally divided into two main categories, i.e., non-generative and generative [13]. For non-generative methods, researchers protect data privacy by perturbing the real trajectory [18], [30], [31] or combining different real trajectories [32]. Although adding random or Gaussian perturbations to the real trajectory contributes to protecting its privacy, these techniques compromise the utility of the data by altering the original spatial-temporal characteristics and data distribution. In addition, it is challenging to strike a compromise between trajectory utility and privacy protection [13]. Mehmet *et al.* generated forged trajectories by mixing several different trajectories, but this work relies on massive data and sophisticated mixing processes [32].

The principle of the generation method is to leverage deep neural networks that learn the spatial-temporal distribution underlying the real data. New trajectory data are therefore generated by sampling from the learned distribution. Liu *et al.* proposed a preliminary solution that employs generative adversarial networks (GAN) for trajectory generation, yet it failed to go further towards a detailed design [33]. Subsequently, some works divided the city map into grids and performed trajectory generation by learning the distribution of trajectories among the grids [4], [12]. However,

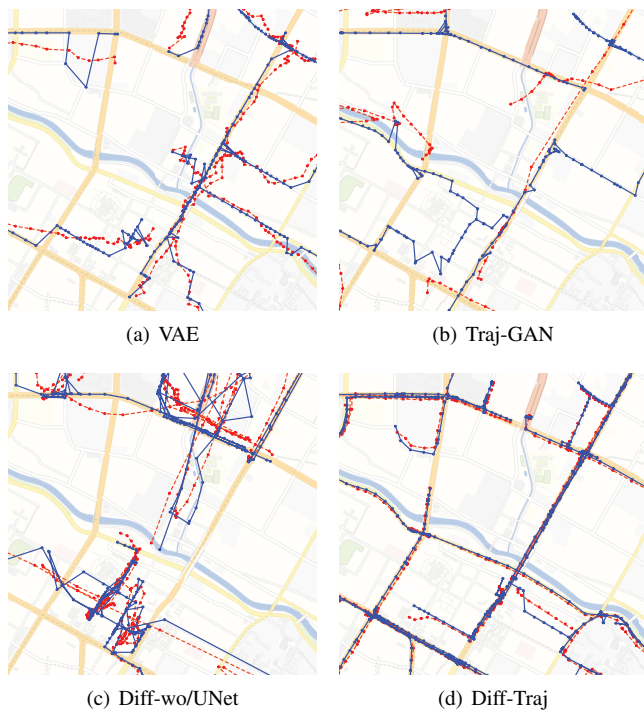


Fig. 9. Forged trajectories map matching result (Red dashed line – generated; blue line – matched).

there is a trade-off between generation accuracy and grid size. Meanwhile, researchers used the image generation capability of GAN to convert the trajectory data into images for time-series generation [13], [14], while the transformation between images and trajectories imposed an additional computational burden. Compared with previous methods, Diff-Traj uses the diffusion model for trajectory generation, which can better explore the spatial and temporal distributions without additional data manipulation.

Diffusion Model The diffusion model is a probabilistic generative model, which was first proposed by Sohl-Dickstein *et al.* [34] and then further improved by Ho *et al.* [15] and Song *et al.* [35]. A typical diffusion model generates synthetic data via two sequential processes, i.e., a forward process that gradually perturbs the data distribution by adding noise on multiple scales and a reverse process that learns how to recover the data distribution [17]. In addition, researchers have made extensive attempts to improve generative sample quality and sampling speed. For example, Song *et al.* proposed a non-Markovian diffusion process to reduce the sampling steps [16], Nichol *et al.* proposed to learn the variance of reverse processes allowing fewer sampling steps [36], and Dhariwal *et al.* searched for the optimal structure of the reverse denoising neural network to obtain better sampling quality. As a new type of advanced generative model, diffusion models have achieved superior performance over alternative generative models in various generative tasks, such as computer vision [37], [38], natural language processing [39], [40], and multi-modal learning [41], [42]. Nevertheless, the diffusion model calls for efforts in spatial-temporal trajectory data generation. To the best of our knowledge, this work is a pioneering attempt that uses diffusion models to generate GPS trajectory.

6 CONCLUSION

In this work, we propose a new GPS trajectory generation method based on diffusion model and spatial-temporal data mining techniques. This method, named Diff-Traj, leverages the data generation ability of the diffusion model and learning from spatial-temporal features by Traj-UNet. Specifically, real trajectories are gradually transformed into random noise by a forward trajectory noising process. After that, Diff-Traj adopts a reverse trajectory denoising process to recover forged trajectories from the noise. Throughout the Diff-Traj framework, we develop a Traj-UNet structure to extract trajectory features and estimate noise levels for the reverse process. Extensive experiments validate the effectiveness of Diff-Traj and its integrated Traj-UNet. Further experiments prove that the data forged by Diff-Traj can conform to the statistical properties of the real trajectory while ensuring utility.

REFERENCES

- [1] Y. Zheng, L. Zhang, X. Xie, and W.-Y. Ma, “Mining interesting locations and travel sequences from gps trajectories,” in *Proceedings of the 18th international conference on World wide web*, 2009, pp. 791–800.
- [2] Y. Zheng, “Trajectory data mining: an overview,” *ACM Transactions on Intelligent Systems and Technology (TIST)*, vol. 6, no. 3, pp. 1–41, 2015.
- [3] Y. Zheng, L. Capra, O. Wolfson, and H. Yang, “Urban computing: concepts, methodologies, and applications,” *ACM Transactions on Intelligent Systems and Technology (TIST)*, vol. 5, no. 3, pp. 1–55, 2014.
- [4] J. Zhang, Q. Huang, Y. Huang, Q. Ding, and P.-W. Tsai, “Dp-trajgan: A privacy-aware trajectory generation model with differential privacy,” *Future Generation Computer Systems*, 2022.
- [5] Y. Zhu, Y. Ye, Y. Liu, and J. J. Yu, “Cross-area travel time uncertainty estimation from trajectory data: a federated learning approach,” *IEEE Transactions on Intelligent Transportation Systems*, vol. 23, no. 12, pp. 24 966–24 978, 2022.
- [6] X. Song, H. Kanasugi, and R. Shibasaki, “Deepttransport: Prediction and simulation of human mobility and transportation mode at a citywide level,” in *Proceedings of the Twenty-Fifth International Joint Conference on Artificial Intelligence*, 2016, pp. 2618–2624.
- [7] Y. Yuan, J. Ding, H. Wang, D. Jin, and Y. Li, “Activity trajectory generation via modeling spatiotemporal dynamics,” in *Proceedings of the 28th ACM SIGKDD Conference on Knowledge Discovery and Data Mining*, 2022, pp. 4752–4762.
- [8] M. Luca, G. Barlacchi, B. Lepri, and L. Pappalardo, “A survey on deep learning for human mobility,” *ACM Computing Surveys (CSUR)*, vol. 55, no. 1, pp. 1–44, 2021.
- [9] Y. Hong, H. Martin, and M. Raubal, “How do you go where? improving next location prediction by learning travel mode information using transformers,” in *Proceedings of the 30th International Conference on Advances in Geographic Information Systems*, 2022, pp. 1–10.
- [10] A. Monreale, F. Pinelli, R. Trasarti, and F. Giannotti, “Wherenext: a location predictor on trajectory pattern mining,” in *Proceedings of the 15th ACM SIGKDD international conference on Knowledge discovery and data mining*, 2009, pp. 637–646.
- [11] Q. Liu, S. Wu, L. Wang, and T. Tan, “Predicting the next location: A recurrent model with spatial and temporal contexts,” in *Thirtieth AAAI conference on artificial intelligence*, 2016.
- [12] K. Ouyang, R. Shokri, D. S. Rosenblum, and W. Yang, “A non-parametric generative model for human trajectories,” in *IJCAI*, vol. 18, 2018, pp. 3812–3817.
- [13] C. Cao and M. Li, “Generating mobility trajectories with retained data utility,” in *Proceedings of the 27th ACM SIGKDD Conference on Knowledge Discovery & Data Mining*, 2021, pp. 2610–2620.
- [14] X. Wang, X. Liu, Z. Lu, and H. Yang, “Large scale gps trajectory generation using map based on two stage gan,” *Journal of Data Science*, vol. 19, no. 1, pp. 126–141, 2021.
- [15] J. Ho, A. Jain, and P. Abbeel, “Denoising diffusion probabilistic models,” *Advances in Neural Information Processing Systems*, vol. 33, pp. 6840–6851, 2020.
- [16] J. Song, C. Meng, and S. Ermon, “Denoising diffusion implicit models,” *arXiv preprint arXiv:2010.02502*, 2020.
- [17] L. Yang, Z. Zhang, Y. Song, S. Hong, R. Xu, Y. Zhao, Y. Shao, W. Zhang, B. Cui, and M.-H. Yang, “Diffusion models: A comprehensive survey of methods and applications,” *arXiv preprint arXiv:2209.00796*, 2022.

- [18] F. Liu, D. Wang, and Z.-Q. Xu, "Privacy-preserving travel time prediction with uncertainty using gps trace data," *IEEE Transactions on Mobile Computing*, pp. 1–1, 2021.
- [19] A. Q. Nichol and P. Dhariwal, "Improved denoising diffusion probabilistic models," in *International Conference on Machine Learning*. PMLR, 2021, pp. 8162–8171.
- [20] O. Ronneberger, P. Fischer, and T. Brox, "U-net: Convolutional networks for biomedical image segmentation," in *International Conference on Medical image computing and computer-assisted intervention*. Springer, 2015, pp. 234–241.
- [21] A. Vaswani, N. Shazeer, N. Parmar, J. Uszkoreit, L. Jones, A. N. Gomez, Ł. Kaiser, and I. Polosukhin, "Attention is all you need," *Advances in neural information processing systems*, vol. 30, 2017.
- [22] Z. Wang, K. Fu, and J. Ye, "Learning to estimate the travel time," in *Proceedings of the 24th ACM SIGKDD International Conference on Knowledge Discovery & Data Mining*. London, United Kingdom: Association for Computing Machinery, 2018, p. 858–866.
- [23] W. Dong, J. Zhang, W. Cao, J. Li, and Y. Zheng, "When will you arrive? estimating travel time based on deep neural networks," in *Proceedings of Thirty-Second AAAI Conference on Artificial Intelligence*. New Orleans, Louisiana, USA: AAAI Press, 2018, p. 2500–2507.
- [24] J. Feng, Z. Yang, F. Xu, H. Yu, M. Wang, and Y. Li, "Learning to simulate human mobility," in *Proceedings of the 26th ACM SIGKDD international conference on knowledge discovery & data mining*, 2020, pp. 3426–3433.
- [25] C. Yang and G. Gidofalvi, "Fast map matching, an algorithm integrating hidden markov model with precomputation," *International Journal of Geographical Information Science*, vol. 32, no. 3, pp. 547–570, 2018.
- [26] A. Paszke, S. Gross, S. Chintala, G. Chanan, E. Yang, Z. DeVito, Z. Lin, A. Desmaison, L. Antiga, and A. Lerer, "Automatic differentiation in PyTorch," in *Advances in Neural Information Processing Systems*, Long Beach, CA, USA, 2017.
- [27] C.-Y. Liou, W.-C. Cheng, J.-W. Liou, and D.-R. Liou, "Autoencoder for words," *Neurocomputing*, vol. 139, pp. 84–96, 2014.
- [28] I. Goodfellow, J. Pouget-Abadie, M. Mirza, B. Xu, D. Warde-Farley, S. Ozair, A. Courville, and Y. Bengio, "Generative adversarial nets," in *Advances in Neural Information Processing Systems*, vol. 27, 2014.
- [29] S. Ruan, C. Long, J. Bao, C. Li, Z. Yu, R. Li, Y. Liang, T. He, and Y. Zheng, "Learning to generate maps from trajectories," in *Proceedings of the AAAI conference on artificial intelligence*, vol. 34, no. 01, 2020, pp. 890–897.
- [30] M. P. Armstrong, G. Rushton, and D. L. Zimmerman, "Geographically masking health data to preserve confidentiality," *Statistics in medicine*, vol. 18, no. 5, pp. 497–525, 1999.
- [31] P. A. Zandbergen, "Ensuring confidentiality of geocoded health data: assessing geographic masking strategies for individual-level data," *Advances in medicine*, vol. 2014, 2014.
- [32] M. E. Nergiz, M. Atzori, and Y. Saygin, "Towards trajectory anonymization: a generalization-based approach," in *Proceedings of the SIGSPATIAL ACM GIS 2008 International Workshop on Security and Privacy in GIS and LBS*, 2008, pp. 52–61.
- [33] L. Xi, C. Hanzhou, and A. Clio, "trajgans: using generative adversarial networks for geo-privacy protection of trajectory data," *Vision paper*, 2018.
- [34] J. Sohl-Dickstein, E. Weiss, N. Maheswaranathan, and S. Ganguli, "Deep unsupervised learning using nonequilibrium thermodynamics," in *International Conference on Machine Learning*. PMLR, 2015, pp. 2256–2265.
- [35] Y. Song, J. Sohl-Dickstein, D. P. Kingma, A. Kumar, S. Ermon, and B. Poole, "Score-based generative modeling through stochastic differential equations," *arXiv preprint arXiv:2011.13456*, 2020.
- [36] A. Nichol, P. Dhariwal, A. Ramesh, P. Shyam, P. Mishkin, B. McGrew, I. Sutskever, and M. Chen, "Glide: Towards photorealistic image generation and editing with text-guided diffusion models," *arXiv preprint arXiv:2112.10741*, 2021.
- [37] R. Rombach, A. Blattmann, D. Lorenz, P. Esser, and B. Ommer, "High-resolution image synthesis with latent diffusion models," in *Proceedings of the IEEE/CVF Conference on Computer Vision and Pattern Recognition*, 2022, pp. 10 684–10 695.
- [38] H. Li, Y. Yang, M. Chang, S. Chen, H. Feng, Z. Xu, Q. Li, and Y. Chen, "Srdiff: Single image super-resolution with diffusion probabilistic models," *Neurocomputing*, vol. 479, pp. 47–59, 2022.
- [39] X. L. Li, J. Thickstun, I. Gulrajani, P. Liang, and T. B. Hashimoto, "Diffusion-lm improves controllable text generation," *arXiv preprint arXiv:2205.14217*, 2022.
- [40] S. Gong, M. Li, J. Feng, Z. Wu, and L. Kong, "Diffuseq: Sequence to sequence text generation with diffusion models," *arXiv preprint arXiv:2210.08933*, 2022.
- [41] O. Avrahami, D. Lischinski, and O. Fried, "Blended diffusion for text-driven editing of natural images," in *Proceedings of the IEEE/CVF Conference on Computer Vision and Pattern Recognition*, 2022, pp. 18 208–18 218.
- [42] A. Ramesh, P. Dhariwal, A. Nichol, C. Chu, and M. Chen, "Hierarchical text-conditional image generation with clip latents," *arXiv preprint arXiv:2204.06125*, 2022.

APPENDIX

We evaluate the model performance of Diff-Traj and baselines on two datasets with different cities, **Chengdu** and **Xi'an**¹. Fig. 10 shows the trajectory distribution and heat map of these two datasets, where the deeper color indicates the more concentrated trajectory in the region. For all datasets, we randomly select all trajectories with lengths greater than 120 for model training and use them to calculate all metrics and generate the distribution of trajectories.

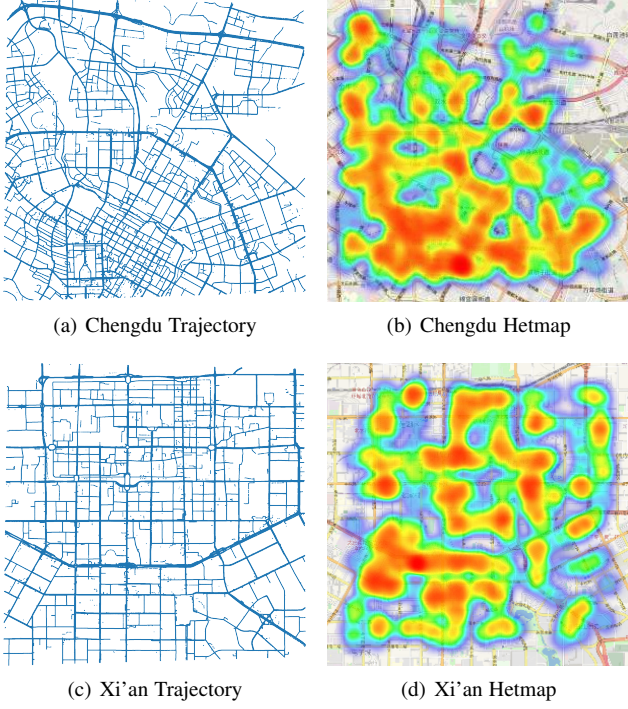


Fig. 10. Origin trajectory distribution of two cities.

For our proposed Diff-Traj framework, we summarize the adopted hyperparameter settings in Table 2. For the training and sampling phase of the proposed framework, we summarize in Algorithm 2 and Algorithm 3, respectively.

TABLE 2
Hyperparameters setting for Diff-Traj.

Hyperparameter	Setting value
Diffusion Steps	300
Skip steps	6
β (linear)	0.0001–0.05
Batch size	2048
Sampling blocks	4
Resnet blocks	2

In this section, we introduce the implementation of baseline methods.

- **Random Perturbation (RP):** We generate -0.01 – 0.01 random noise to perturb the original trajectory. This degree of noise ensures that the maximum distance between the perturbed points and the original does not exceed 2 km

1. These datasets can be downloaded (following approval of access request) at <https://outreach.didichuxing.com/>

Algorithm 2: Diffusion Training Phase

```

1: for  $i = 1, 2, \dots$ , do
2:   Sample  $\mathbf{x}_0 \sim q(\mathbf{x})$ ,
3:    $t \sim \text{Uniform}\{1, \dots, T\}$ 
4:    $\epsilon \sim \mathcal{N}(0, \mathbf{I})$ 
5:    $\mathcal{L} = \|\epsilon - \epsilon_\theta(\sqrt{\alpha_t}\mathbf{x}_0 + \sqrt{1 - \alpha_t}\epsilon, t)\|^2$ 
6:    $\theta = \theta - \eta \nabla_\theta \mathcal{L}$ 
7: end for

```

Algorithm 3: Diffusion Sampling Phase

```

1: Sample  $\mathbf{x}_T \sim \mathcal{N}(0, \mathbf{I})$ 
2: for  $t = T, T-1, \dots, 1$  do
3:   Compute  $\mu_\theta(\mathbf{x}_t, t)$  according to Eq. (12)
4:   Compute  $p_\theta(\mathbf{x}_{t-1} | \mathbf{x}_t)$  according to Eq. (13)
5: end for
6: return  $\mathbf{x}_0$ 

```

- **Gaussian Perturbation (GP):** We generate Gaussian noise perturbed original trajectories with mean 0 and variance 0.01.
- **Variational AutoEncoder (VAE) [27]:** In this work, trajectories are first embedded as a hidden distribution through two consecutive convolutional layers and a linear layer. Then, we generate the trajectories by a decoder consisting of a linear layer and two deconvolutional layers. The size of convolution kernels in convolutional and deconvolutional layers is set to 4 to ensure that input and output trajectories have the same size.
- **TrajGAN [28]:** The trajectory is first combined with random noise and then passes through a generator consisting of two linear layers and two deconvolution layers. Subsequently, a convolutional layer and a linear layer are adopted as the discriminator. The generator and the discriminator are trained in an alternating manner.
- **Diff-scatter:** We randomly sample GPS scatter points from trajectories and generate scatter points using a 4-layer MLP (neurons: $\{128, 256, 256, 128\}$) and the diffusion model.
- **Diff-wo/Traj-UNet:** The model uses only two Resnet blocks combined with a single attention layer between them.

We append a series of experimental results in this section due to space constraints. Fig. 11 shows the geographic results of the trajectories generated by different generation methods in Xi'an. The rest visualize the forward trajectory addition noise process and reverse trajectory denoising process of Diff-Traj.

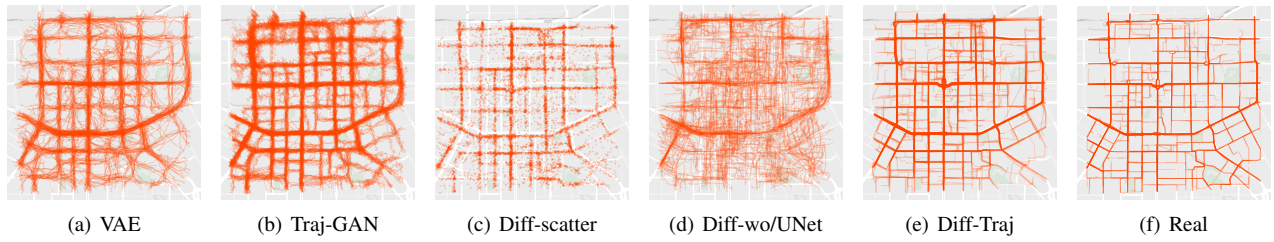


Fig. 11. Comparison of forged trajectory in Xi'an.

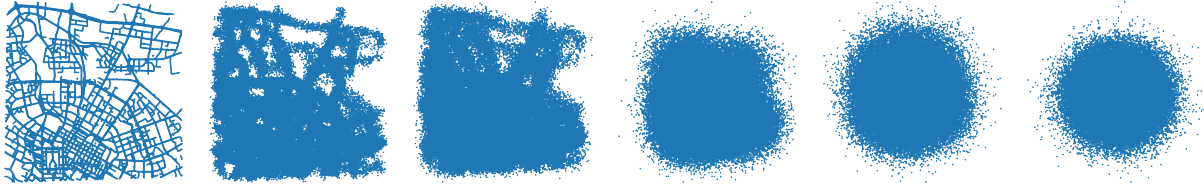


Fig. 12. Forward trajectory noising process (Chengdu).

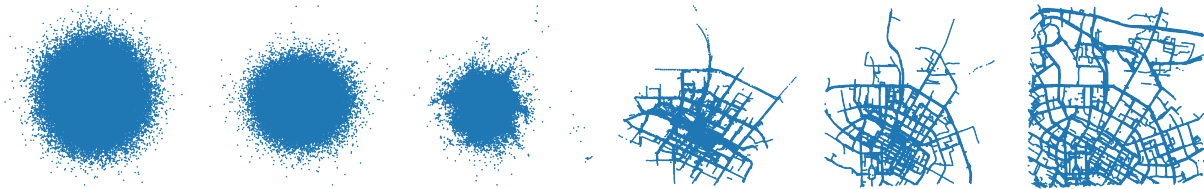


Fig. 13. Reverse trajectory denoising process (Chengdu).



Fig. 14. Forward trajectory noising process (Xi'an).

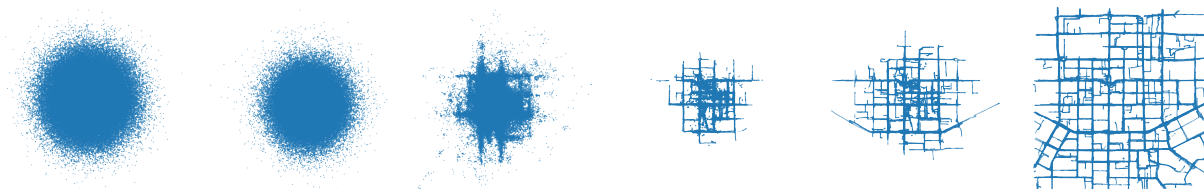


Fig. 15. Reverse trajectory denoising process (Xi'an).